EC
Journals.ASM.org

Vacuolar H^+-ATPase Works in Parallel with the HOG Pathway To Adapt *Saccharomyces cerevisiae* Cells to Osmotic Stress

Sheena Claire Li, Theodore T. Diakov, Jason M. Rizzo, and Patricia M. Kane

Department of Biochemistry and Molecular Biology, SUNY Upstate Medical University, Syracuse, New York, USA

Hyperosmotic stress activates an array of cellular detoxification mechanisms, including the high-osmolarity glycerol (HOG) pathway. We report here that vacuolar H^+-ATPase (V-ATPase) activity helps provide osmotic tolerance in *Saccharomyces cerevisiae*. V-ATPase subunit genes exhibit complex haploinsufficiency interactions with HOG pathway components. *vma* mutants lacking V-ATPase function are sensitive to high concentrations of salt and exhibit Hog1p activation even at low salt concentrations, as demonstrated by phosphorylation of Hog1p, a shift in Hog1-green fluorescent protein localization, transcriptional activation of a subset of HOG pathway effectors, and transcriptional inhibition of parallel mitogen-activated protein kinase pathway targets. *vma2*Δ *hog1*Δ and *vma3*Δ *pbs2*Δ double mutants have a synthetic growth phenotype, poor salt tolerance, and an aberrant, hyper-elongated morphology on solid media, accompanied by activation of a filamentous response element-LacZ construct, indicating cross talk into the filamentous growth pathway. Vacuoles isolated from wild-type cells briefly exposed to salt show higher levels of V-ATPase activity, and Na^+/H^+ exchange in isolated vacuolar vesicles suggests a biochemical basis for the genetic interactions observed. V-ATPase activity is upregulated during salt stress by increasing assembly of the catalytic V_1 sector with the membrane-bound V_o sector. Together, these data suggest that the V-ATPase acts in parallel with the HOG pathway in order to mediate salt detoxification.

The adaptation to extracellular stress is an absolute requirement for survival. At the most basic level, the hyperosmotic stress response has been studied in unicellular organisms such as *Saccharomyces cerevisiae* as a model for how the cell senses extracellular stress, transmits signals from receptors at the plasma membrane, and triggers signaling cascades within the cell that lead to changes in gene expression and protein function (17). The cellular responses to hyperosmotic stress are highly conserved, and the basic principles learned from budding yeast and other model organisms have proven to be applicable to more complex species. In mammalian systems, cells that are exposed to ionic flux (i.e., renal cells) must have robust hyperosmotic stress mechanisms in place. In plants, salt detoxification is critically important for the growth of crops in arid environments, and responses to salt stress have been studied extensively (35, 42, 44).

Salt shock involves an uncharged osmotic component, as well as an ionic component (17, 44). In high-salt environments, water rushes out of the cell, while sodium and chloride ions enter. The resulting change in water potential and ion imbalance disrupts fundamental cellular processes. The canonical response to salt/hyperosmotic shock in eukaryotes is the activation of the high-osmolarity glycerol (HOG) pathway. The HOG pathway is a mitogen-activated protein kinase (MAPK) cascade that, when activated, results in both transcriptional and nontranscriptional responses (17). The HOG pathway confers osmotolerance by increasing the amount of intracellular solute to prevent the efflux of water from the cell and by activating plasma membrane cation transporters that export excess ions out of the cytoplasm. These dynamic changes are accompanied by controlled cell cycle arrest and the modulation of translational efficiency (17, 47).

Aside from HOG pathway activation, there are other changes that take place in yeast cells upon osmotic shock. Vacuolar fragmentation in response to salt stress increases the surface/volume ratio of the vacuole, and this may allow maximal sequestration of cations into the vacuole by transporters (3, 10–12, 22, 24, 45). Calcium release from the vacuole also accompanies osmotic shock (8). This results in a transient increase in the cytosolic concentration of Ca^{2+}, which in turn activates the Ca^{2+}/calmodulin/calcineurin signaling pathway (6). The presence of these responses at the vacuole suggests that this organelle is important for salt detoxification and tolerance to hyperosmotic stress.

The vacuolar H^+-ATPase is a ubiquitous proton pump that acidifies intracellular compartments and, in specific scenarios, transports protons across the plasma membrane (20). Structurally homologous, though functionally distinct, from the F_1F_0 ATP synthase, the vacuolar proton-translocating ATPase (V-ATPase) is composed of two multi-subunit sectors and couples energy from ATP hydrolysis (the V_1 sector) to the transport of protons against transmembrane gradients (the V_o sector). From yeast to humans, V-ATPases acidify a series of endocytic compartments terminating at the vacuole/lysosome, the most acidic organelle. V-ATPases also acidify compartments of the biosynthetic pathway such as the late Golgi apparatus and secretory vesicles. The maintenance of these acidic compartments is crucial for trafficking in both the endocytic and the biosynthetic pathways, macromolecule degradation and recycling, and ion homeostasis. At the vacuolar membrane, the pH gradient generated by the V-ATPase energizes transporters to drive the uptake of ions and amino acids into the vacuolar lumen (24).

Deleting any subunit of the V-ATPase completely inactivates the enzyme, and genetic loss of the V-ATPase is lethal in meta-

Received 5 August 2011 **Accepted** 22 December 2011
Published ahead of print 30 December 2011
Address correspondence to Patricia M. Kane, kanepm@upstate.edu.
Supplemental material for this article may be found at http://ec.asm.org/.

doi:10.1128/EC.05198-11

TABLE 1 Genotypes of yeast strains used in this study

Strain	Genotype	Source or reference
BY4741 (wild type)	*MAT***a** *his3*Δ*1 leu2*Δ*0 met15*Δ*0 ura3*Δ*0*	Open Biosystems
BY4742 (wild type)	*MAT*α *his3*Δ*1 leu2*Δ*0 lys2*Δ*0 ura3*Δ*0*	Open Biosystems
BY4741*vma2*Δ	*MAT***a** *his3*Δ*1 leu2*Δ*0 met15*Δ*0 ura3*Δ*0 vma2*Δ::*kanMx*	Open Biosystems
BY4741*hog1*Δ	*MAT***a** *his3*Δ*1 leu2*Δ*0 met15*Δ*0 ura3*Δ*0 hog1*Δ::*kanMx*	Open Biosystems
BY4741*vma2*Δ*hog1*Δ	*MAT***a** *his3*Δ*1 leu2*Δ*0 met15*Δ*0 ura3*Δ*0 vma2*Δ::*natR hog1*Δ::*kanMx*	This study
BY4741*vma3*Δ*pbs2*Δ	*MAT***a** *his3*Δ*1 leu2*Δ*0 met15*Δ*0 ura3*Δ*0 vma3*Δ::*natR pbs2*Δ::*kanMx*	This study
BY4741*vma13*Δ::Nat^{R}α	*MAT*α *his3*Δ*1 leu2*Δ*0 lys2*Δ*0 ura3*Δ*0 vma13*Δ::*natR*	Rizzo et al. (37)
SF838-5aα (wild type)	*MAT*α *leu3-2,112 ura3-52 ade6 gal2*	Tom Stevens

zoans. In yeast, V-ATPase gene deletion mutants (*vma* mutants) are viable when grown in moderately acidic media (pH 5.0) but are unable to grow in alkaline conditions with elevated calcium (pH 7.5, 100 mM $CaCl_2$) (41). This is known as the Vma$^-$ phenotype. The *VMA13* gene encodes a V_1 sector subunit required for activity but not assembly of the enzyme. Diploid *vma13*Δ hemizygotes (*VMA13/vma13*Δ) mimic the growth defect of *vma* mutants: they are unable to grow in media with elevated pH and calcium levels (37). Interestingly, the haploinsufficiency phenotype of the *VMA13/vma13*Δ hemizygote is worsened by adding a second heterozygous deletion of *VMA3*, a V_o sector subunit. Diploids with compound hemizygous deletions of both *vma13* and *vma3* have severe growth defects, a complete absence of V-ATPase activity at the vacuole, and elevated levels of ATP hydrolysis by cytosolic V_1 complexes (37). This is a complex haploinsufficiency (CHI) phenotype, where haploid copy numbers of two different genes are insufficient for normal cell growth or viability in a diploid (15).

We hypothesized that heterozygous V-ATPase subunit mutations might also show CHI interactions with mutations in other processes that require full V-ATPase activity. A full genomic CHI screen could thus provide insights into novel physiological functions of the V-ATPase. To test this hypothesis, we screened for haploid deletion mutants that, when mated to the haploid *vma13*Δ mutant, had more severe growth defects than the *VMA13/vma13*Δ strain. From this screen, we found that V-ATPase and HOG pathway genes interact genetically in *Saccharomyces cerevisiae*. This initial data led us to further pursue the functional link between the V-ATPase and the HOG pathway; we discovered that the loss of V-ATPase activity leads to constant low-level activation of the HOG pathway and that the V-ATPase itself is a salt-activated enzyme in yeast.

MATERIALS AND METHODS

Media. Yeast extract-peptone-dextrose (YPD) was prepared as described previously (1) and buffered to pH 5.0 with 50 mM potassium phosphate and 50 mM potassium succinate. Supplemented minimal medium and 5-fluoroorotic acid (FOA)-containing media were prepared as described previously (1). ClonNat (Nat) and G418 antibiotics were added at a concentration of 200 μg/ml.

Yeast strains and plasmids. Wild-type yeast strains BY4741 and BY4742 and the congenic *vma*Δ mutants used were part of a yeast deletion mutant array purchased from Research Genetics/Open Biosystems. Their genotypes are indicated in Table 1. Plasmids were introduced into haploid deletions strains using an overnight lithium acetate transformation protocol (13). Transformants were selected on supplemented minimal medium lacking uracil (SD-uracil).

CHI screen. To screen for genes that have a CHI interaction with *vma13*Δ or *vma3*Δ, we adapted a methodology previously described (15) with some minor modifications (Fig. 1A). The EUROSCARF collection of nonessential yeast deletion mutants arrayed in a 384-colony/plate format was used. This library is an ordered array of ~4,800 haploid strains, each with a nonessential gene deleted by replacement of the gene's open reading frame with the G418/kanamycin resistance gene (G418^R) (14). The *vma13*Δ::Nat^R query strain was generated with a Nat^R (nourseothricin) resistance gene replacing the *VMA13* open reading frame (46). The query strain was mated to the EUROSCARF collection (*yfg*::*kanMx*) using a Virtek Colony Arrayer. Diploids were selected on YPD+Nat+G418 medium and allowed to grow for 24 h at 30°C. To prevent unwanted compensatory mechanisms caused by the deletion of the V-ATPase, the query strain was transformed prior to mating with a CEN-linked plasmid expressing wild-type *VMA13* (*VMA13-YCp50*). The diploids were then spotted onto plates with 5-fluoroorotic acid (5-FOA; supplemented minimal medium containing 5-FOA, Nat, and G418) to select against the plasmid. Mutants that grew poorly on the 5-FOA plates were compared to control plates (supplemented minimal medium plus Nat plus G418 with no FOA) after 48 h of growth at 30°C. The strains which grew more poorly in the presence of FOA were scored as having complex haploinsufficiency (CHI) interactions with the *vma13*Δ mutant. Similar procedures were followed for the *vma3*Δ CHI screen and a full list of interactors is shown in Table S1 in the supplemental material.

To confirm the hits, we obtained from the genomic CHI screen, we manually mated the haploid yeast strain with the *vma13* deletion (*vma13*Δ::Nat^R *MAT*α) initially masked with a VMA13-YCp50 plasmid to strains that we found as hits from the genomic screen (*yfg*Δ::*kanMx MAT***a**; *yfg* refers to any gene which was deleted in a particular hit). The selected diploids were then plated on FOA medium to select for cells which have lost the plasmid, and their growth phenotypes were evaluated as described above.

Activation of Hog1p. For visualization of Hog1 phosphorylation by immunoblotting, wild-type and *vma2*Δ cells were grown to mid-log phase (A_{600}/ml = 0.5) in synthetic complete medium. For each sample, portions equivalent to 5 optical density units were pelleted by centrifugation, and resuspended in supplemented minimal medium without salt or with increasing concentrations of NaCl as indicated. Cells were incubated for 10 min at 30°C and pelleted in a tabletop centrifuge. The pellets were resuspended in 100 μl of cracking buffer (8 M urea, 5% sodium dodecyl sulfate [SDS], 1 mM EDTA, 50 mM Tris-HCl [pH 6.8], 5% β-mercaptoethanol) at 95°C for 5 min. For visualization of nuclear localization of Hog1p, a BY4741 wild-type strain containing Hog1 C-terminally tagged with green fluorescent protein (GFP) were purchased from Invitrogen. This strain was transformed with a *vma2*Δ::Nat^R allele (37) to obtain a BY4741 *vma2*Δ strain containing *HOG1-GFP*. For visualization of Hog1-GFP localization, wild-type and *vma2*Δ strains were grown to log phase in supplemented minimal medium, concentrated by brief centrifugation, and resuspended in fresh medium. The strains were then visualized directly (no salt) or incubated at 30°C for 10 min with 0.1 M NaCl before placement on the slide. The salt-treated cells were viewed and photographed over the next 10 min. Fluorescence was visualized by using a GFP filter set, and all photographs of GFP fluorescence were taken using the same exposure.

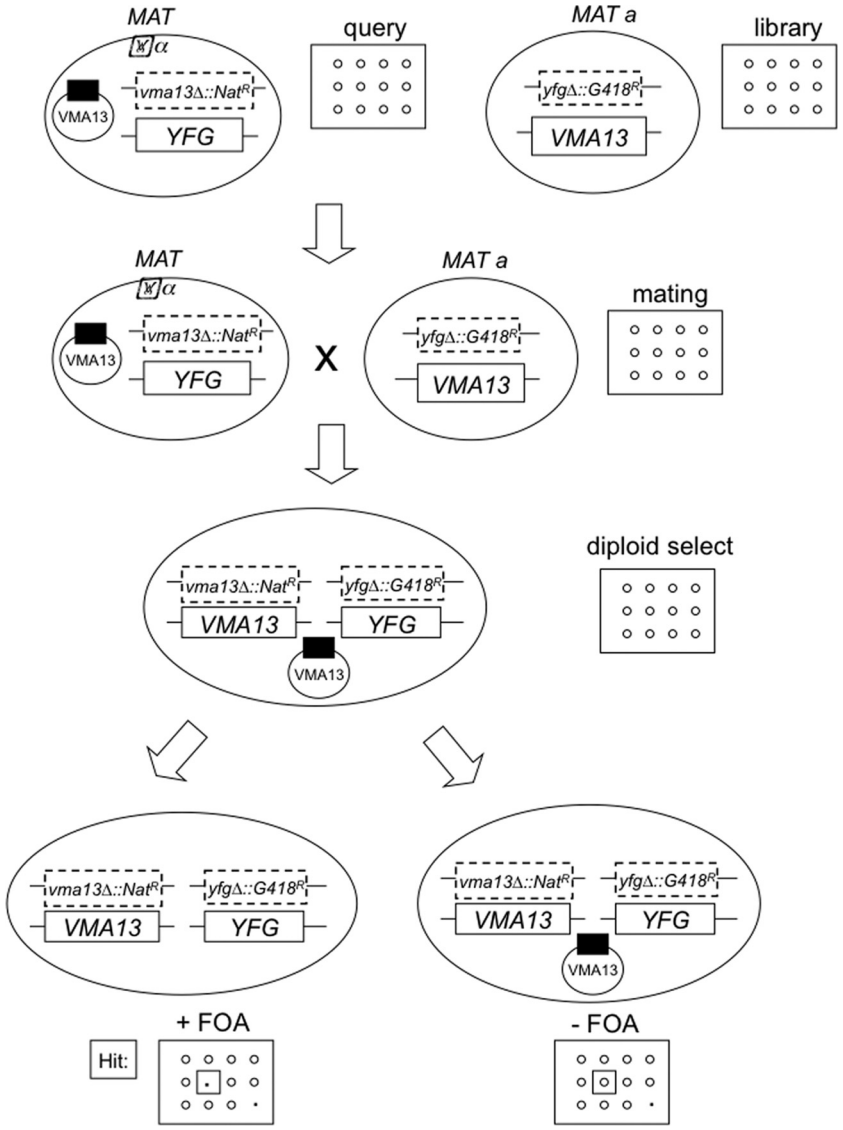

FIG 1 CHI scheme. All cell manipulations were performed using a Virtek colony arrayer. *vma13*Δ::Nat^R haploids were transformed with a plasmid containing the wild-type *VMA13* gene and a *URA3* marker to initially mask the effects of the *vma13* deletion. These haploids were mated to a library of nonessential yeast deletion mutants (*yfg*Δ::G418^R). Diploids heterozygous for both the *vma13*Δ and the *yfg*Δ mutations were selected on medium containing G418+Nat. The diploids were then spotted onto plates with 5-fluoroorotic acid (5-FOA + Nat + G418) to uncover the *vma13*Δ::Nat^R/*VMA13* hemizygosity. Mutants that grew more poorly on the 5-FOA plates than on control plates (Nat + G418, no FOA) exhibited complex haploinsufficiency (CHI) with the *vma13*Δ mutant.

Western blotting. For Hog1p activation experiments, 10 μl of each sample was separated by SDS-PAGE. The proteins were immunoblotted onto nitrocellulose, and phosphorylated forms of Hog1p were detected using a phospho-p38 antibody (antibody 3D7; Cell Signaling). As a loading control, total Hog1p was detected using an anti-Hog1 antibody (sc-9079; Santa Cruz Biotechnology). A goat anti-rabbit horseradish peroxidase-conjugated antibody (Pierce) was used as the secondary antibody on the immunoblots. The enhanced chemiluminescence method (GE Healthcare) was used to detect binding. Signals were quantified using NIH ImageJ software.

For the detection of vacuolar protein levels by immunoblotting, vacuolar vesicles were solubilized at 65°C with cracking buffer, separated by SDS-PAGE, and transferred to nitrocellulose. As previously described (25), the mouse monoclonal antibodies 8B1, 13D11, 7A2, and 10D7 were used to detect V-ATPase subunits A, B, C, and a, respectively.

Growth curves. Wild-type cells, *vma*Δ mutants, *hog*Δ mutants, and *vma*Δ *hog*Δ double mutants were grown at 30°C in YPD (pH 5.0) to mid-log phase (A_{600}/ml = 0.5). Portions (10 μl) of these cultures were transferred into multiwell plates containing 600 μl of YPD (pH 5.0) containing 0 to 1.0 M NaCl. Growth curves over 48 h were determined using an automated plate reader (Infinite F200; Tecan).

Microscopy. Light microscopy was performed using an epifluorescence microscope (Imager-Z1; Zeiss). To compare the morphologies of wild-type, *vma*Δ, *hog*Δ, and *vma*Δ *hog*Δ strains, the cells of each respective genotype were grown on YPD (pH 5.0) plates at 30°C for 48 h. Single colonies were taken from these plates and placed in 5 μl of YPD (pH 5.0) on a microscope slide.

Analysis of pFRE-LacZ activation. Filamentous growth pathway activation was observed using a filamentous response element (FRE)-*lacZ* reporter gene. Yeast strains (i.e., wild-type, *vma3*Δ, *hog1*Δ, and *vma3*Δ *pbs2*Δ strains) were transformed with a FRE-*lacZ*-bearing 2μ plasmid, obtained from Paul Cullen (SUNY Buffalo) (32). To assess the activation of the FRE-LacZ construct, transformants were maintained on solid medium and suspended for determination of the optical density, and

LacZ expression was measured using an ONPG (*o*-nitrophenyl-β-D-galactopyranoside) assay (40). The assay was performed as described earlier, except that the cell pellet from ~0.6 OD_{600} units of cell suspension was resuspended in 150 μl of Z-buffer containing 0.27% 2-mercaptoethanol and then 50 μl of chloroform and 20 μl of 0.1% SDS were added. After vortex mixing for 15 s, the reaction was initiated by adding 700 μl of a 1-mg/ml dilution of ONPG in Z-buffer containing 2-mercaptoethanol. The rate of the reaction was monitored over the next 30 to 45 min at 30°C as described previously (40).

Purification of vacuolar vesicles and activity assays. Vacuolar vesicles were isolated as previously described (19, 39) with the following modifications. Cells were grown overnight to log phase (A_{600} = 0.6 to 1.0) in synthetic complete medium buffered to pH 5.0 with 50 mM 2-(*N*-morpholino)ethanesulfonic acid. After removal of the cell wall with zymolyase, spheroplasts were washed and resuspended in growth medium buffered to pH 5.0 containing 1.2 M sorbitol. Half of the spheroplasts were exposed to 500 mM sodium chloride at this step, and all cells were recovered for 30 min at 30°C. Subsequent cell lysis and isolation of vacuoles by flotation on Ficoll gradients were performed identically for all samples.

ATP hydrolysis rates were determined on freshly prepared vacuolar vesicles by a coupled enzyme assay as described previously (25). Concanamycin inhibition was measured by adding concanamycin A directly to the assay mixture to a final concentration of 100 nM. The specific V-ATPase activity represents the rate of concanamycin A-sensitive ATPase hydrolysis, expressed as μmol of ATP consumed/min/mg of vacuolar protein.

Proton pumping was observed using the 9-amino-6-chloro-2-methoxyacridine (ACMA) quenching assay described previously (25), with some modifications. Portions (10 μg) of vacuolar vesicles were used for each assay. Pumping was initiated by adding 0.5 mM ATP and 1.0 mM $MgSO_4$ at the 100-s time point. Inhibition of the V-ATPase was achieved by adding concanamycin A at different concentrations (100, 0.25, or 0.5 nM) at the indicated time points. Sodium chloride was added to a final concentration of 333.3 mM at the indicated time points.

RESULTS

CHI interactions between the V-ATPase and members of the HOG pathway. We exploited the phenotype of the *VMA13*/*vma13*Δ hemizygote to screen for other genes that have CHI interactions with *vma13*Δ. To do this, we adapted methodology used in previous genome-wide studies in yeast (15), with some modifications (Fig. 1). In parallel, we also screened for genes that showed CHI interactions with a *vma3*Δ mutation, which disrupts a membrane subunit of the V-ATPase. A list of genes that were identified in at least two of three independent screens with each of the *vma* mutations is shown in Table S1 in the supplemental material, and an analysis of enriched functional and process terms determined using FUNSPEC is provided in Table S2 in the supplemental material. Osmosensing and response was identified as an enriched MIPS functional classification (P = 0.001), and the osmosensory signaling pathway was identified through GO biological process analysis (P = 0.0017). Osmotic sensitivity was the most significantly enriched MIPS phenotype term (P = 0.0019). Two components of the HOG MAPK pathway (*PBS2* and *SSK1*), as well as a negative regulator of this pathway (*PTP2*), were strong hits in the screens. Genomic CHI screens have been reported to have a relatively high rate of false-positive and false-negative interactions (15), so we confirmed CHI interactions between the HOG pathway and the V-ATPase by manually mating *vma13*Δ::Nat^R cells to the main components of the HOG MAPK signaling pathway (Fig. 2B), selecting for diploids, and comparing growth on +FOA versus −FOA media. When several HOG pathway components were individually tested for CHI with *vma13*Δ cells

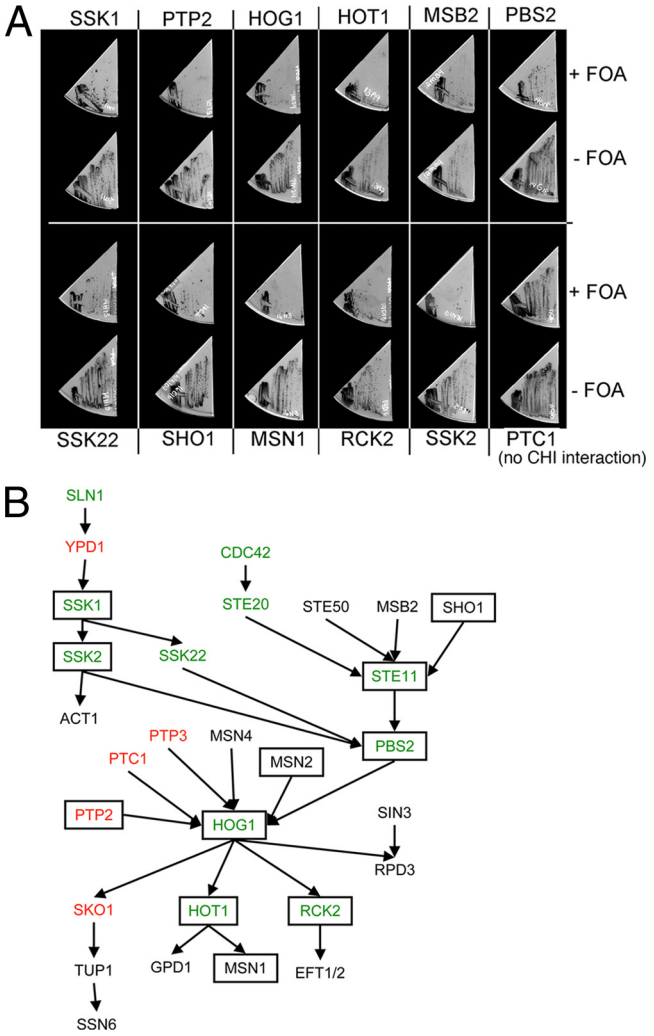

FIG 2 CHI interactions between the V-ATPase and HOG pathway members. (A) Members of the HOG MAPK pathway were retested for CHI interactions with *vma13*Δ. The *vma13*Δ::Nat^R strain was mated to different HOG pathway deletion mutants from the EUROSCARF library. Diploids were selected on rich media containing 200 μM nourseothricin (Nat) and 200 μM G418, and the *vma13*Δ hemizygosity was demonstrated by plating cells on synthetic media lacking uracil that contained 5-FOA, Nat, and G418. "+FOA" and "−FOA" plates were incubated at 30°C for 48 h before scoring. Growth on −FOA but not on +FOA indicates a CHI interaction. Some strains (such as *ssk1*Δ and *pbs2*Δ strains) showed a few isolated colonies on +FOA, but there is much less growth than on −FOA plates; a more complete set of interactions is shown in Fig. S1A in the supplemental material. (B) V-ATPase-HOG CHI network. The HOG MAPK pathway was used as a backbone for this diagram. Positive regulators of the pathway are in green, while negative regulators are in red. Genes that exhibit a CHI interaction with *vma13*Δ mutants are enclosed in rectangles. (Adapted from reference 44a with permission.)

(Fig. 2A), both positive and negative regulators of the pathway (Fig. 2B) exhibited CHI interactions. (Notably, negative regulators of the HOG pathway are coordinately regulated with positive regulators to prevent lethal activation of the pathways [50].) A larger set of CHI interactions is shown in Fig. S1A in the supplemental material; similar results were obtained when screening with a *vma3*Δ mutant and are shown in Fig. S1B in the supplemental material. Upstream activators and inhibitors of the HOG MAPK pathway showed CHI interactions with both *VMA3* and

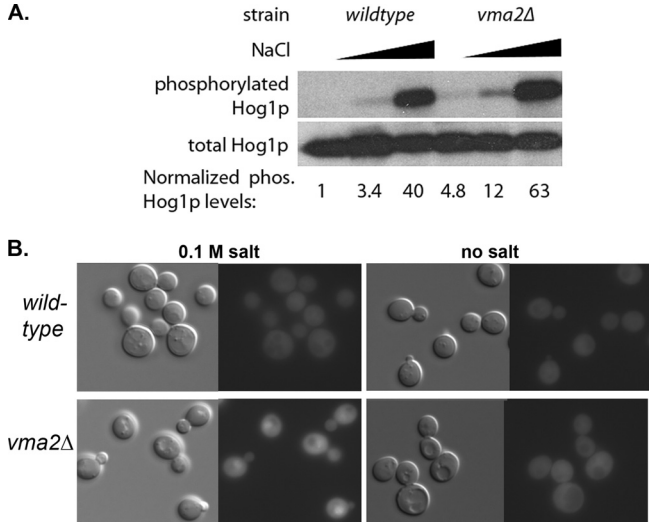

FIG 3 A *vma2*Δ mutant activates the HOG pathway at lower salt concentrations than in wild-type cells. (A) Haploid wild-type and *vma2*Δ cultures were grown to log phase in synthetic complete medium and then pelleted and resuspended with medium containing different NaCl concentrations (no salt, 0.25 M, and 0.5 M) for 5 min at 30°C. An antibody against phosphorylated p38 was used to visualize activated Hog1p on Western blots. Total Hog1 protein was also visualized using an anti-Hog1 antibody. Normalized levels of phosphorylated Hog1 were determined by quantitating intensity of phosphorylated and total Hog1 for each sample using ImageJ, correcting the phosphorylated Hog1 signal for differences in total Hog1 in that sample, and then normalizing to the intensity in the wild-type strain with no added salt. (B) A *HOG1-GFP* construct was integrated into wild-type and *vma2*Δ mutant strains at the *HOG1* locus. Cells were grown to log phase in synthetic complete medium and then visualized directly (right panels) or challenged with 0.1 M NaCl for 10 min at 30°C before placement on the slide and visualization over the next 10 min (left panels). Nomarski images are shown on the left for each set of images, and fluorescence micrographs, obtained under a GFP filter set, are shown on the right. All fluorescent images were obtained under identical exposure times.

VMA13, suggesting that the genetic interaction between the HOG pathway and the V-ATPase was not specific for a particular V-ATPase subunit, but instead reflected a general synthetic growth defect in cells compromised for both HOG pathway activity and V-ATPase function.

The HOG pathway is activated in *vma* mutants. CHI interactions can arise when loss of one process results in a requirement for compensatory activity in the other process. We therefore assessed HOG pathway activity in a *vma2*Δ mutant, which, like *vma13*Δ and *vma3*Δ mutants, has no V-ATPase activity. Phosphorylation of Hog1p is a marker for HOG pathway activation, and we compared Hog1 phosphorylation in wild-type cells to *vma2*Δ cells (Fig. 3A). Both strains were exposed for 10 min to rich medium containing no added NaCl, 0.25 M NaCl, or 0.5 M NaCl. The cells were then lysed, and Hog1p activation was examined by probing immunoblots with antibodies recognizing total Hog1p or phosphorylated Hog1p. As shown in Fig. 3A, there was more phosphorylation of Hog1p in *vma2*Δ mutants than in wild-type cells, particularly under low salt concentrations. Even with no added salt, there is almost five times more Hog1 phosphorylation in the *vma2*Δ mutant than in wild-type cells (where phosphorylated Hog1 is barely detectable), and approximately four times more in *vma2*Δ cells treated with 250 mM NaCl. With a high salt concentration, the Hog1p appears to be fully activated in both strains. These data suggest that hyperactivation of the HOG pathway in the *vma2*Δ mutant may help to compensate for loss of V-ATPase function, particularly in the presence of mild osmotic stress. Activation of Hog1p in response to salt is accompanied by a transient recruitment to the nucleus. Based on the data in Fig. 4A, we hypothesized that Hog1-GFP might be transported into the nucleus at lower salt concentrations in *vma2*Δ mutants than in wild-type cells. As shown in Fig. 4B, Hog1-GFP was mobilized to concentrated areas after treatment of *vma2*Δ cells with 100 mM NaCl, similar to that observed previously for nuclear localization of Hog1-GFP in wild-type cells treated with much higher salt con-

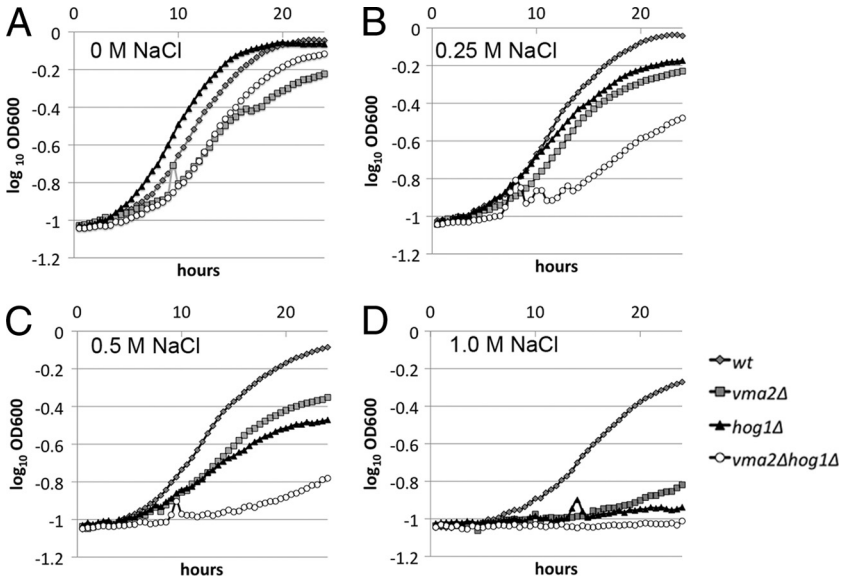

FIG 4 Growth analysis of *vma2*Δ, *hog1*Δ, and *vma2*Δ *hog1*Δ haploids. Growth curves of haploid wild type and *vma2*Δ, *hog1*Δ, and *vma2*Δ *hog1*Δ mutant strains in liquid synthetic complete media containing increasing concentrations of salt (0 M NaCl [A], 0.25 M NaCl [B], 0.5 M NaCl [C], 1.0 M NaCl [D]). Growth was observed over the span of 24 h at 30°C.

centrations (28). The mobilization of Hog1p-GFP fluorescence was transient in vma2Δ cells, appearing ~12 min after salt addition and completely disappearing by 30 min after salt treatment, a finding consistent with previous reports of Hog1 activation (28). Significantly, there was no mobilization of Hog1p in wild-type cells treated with 100 mM salt, although a prominent mobilization of Hog1p was observed when these cells were treated with 1 M NaCl. In addition, treatment of wild-type cells with the V-ATPase inhibitor concanamycin A before challenge with 0.1 M NaCl resulted in Hog1-GFP mobilization (data not shown), again suggesting that in the absence of V-ATPase activity, compensatory HOG pathway activation occurs at low salt concentrations.

Consistent with these results, a previous microarray analysis revealed that a subset of mRNA transcripts of downstream targets of the HOG pathway are upregulated in a *vma2*Δ mutant grown in rich medium with relatively low salt concentrations (see Table S3 in the supplemental material) (29). Among these transcripts were *PTP2*, *GRE1*, *AQY2*, and *SIP18*. Transcripts of *GRE1*, *AQY2*, *SIP18*, and *YML131W* are induced during hyperosmotic conditions. *PTP2* is notable because it is the protein phosphatase that inactivates the HOG pathway during osmolarity sensing, but upregulation of the phosphatase in parallel with HOG pathway activation has been documented previously (18). Activation of the HOG pathway not only results in activation of a number of genes in order to generate proteins that can help cells cope with the stress but also results in the downregulation of a number of genes that are products of other MAPK pathways as a mechanism for inhibiting cross talk between MAPK pathways (7, 30, 36, 38, 43). The genes downregulated by Hog1 are overexpressed in response to salt in a *hog1*Δ mutant and include targets of the mating pathway (*AGA1*, *AGA2*, *MFA1*, FIG 1, *FUS1*, *BAR1*, *ASG7*, and *YNL279W*), as well targets of the filamentous growth pathway (the major regulator *TEC1*) (36). Interestingly, these nine genes are significantly downregulated in the *vma2*Δ mutant, and represent 9 of the 13 targets that are most highly upregulated in response to high salt in a *hog1*Δ mutant, suggesting that they are negatively regulated by the HOG pathway (29, 36) (see Table S4 in the supplemental material). This provides another indication that the HOG pathway is constitutively activated in the *vma2*Δ mutant.

***vma*Δ *hog*Δ double mutants have a synthetic growth and morphology phenotype.** In order to further pursue the interaction between the HOG pathway and V-ATPase, we constructed haploid single and double mutants and analyzed their phenotypes. A set of mutants with single deletions of a HOG pathway gene (*hog1*Δ and *pbs2*Δ) or V-ATPase genes (*vma2*Δ and *vma3*Δ) or double deletions of both HOG and V-ATPase genes (*vma2*Δ *hog1*Δ and *vma3*Δ *pbs2*Δ) were tested for growth in rich media containing different concentrations of NaCl. (Fig. 4 and 5; see also Fig. S2 in the supplemental material). Interestingly, single-deletion mutants of both a V_1 sector subunit (*vma2*Δ, Fig. 4) and a V_o sector subunit (*vma3*Δ, see Fig. S2 in the supplemental material) exhibited impaired growth under high (0.5 to 1.0 M) NaCl concentrations. This salt-sensitive phenotype showed that V-ATPase function is necessary for optimal growth under hyperosmotic stress. A mutant lacking both the HOG and the V-ATPase pathways would conceivably have an even more severe phenotype under these stress conditions. Indeed, *vma2*Δ *hog1*Δ (Fig. 4) and *vma3*Δ *pbs2*Δ (see Fig. S2 in the supplemental material) double mutants grow slowly even under normal (low-salt) conditions. The slow-growth phenotype of the *vma*Δ *hog*Δ double mutants was significantly worsened under relatively low amounts (0.25 M) of NaCl in the growth media, and these double mutants were completely unable to grow under high osmotic stress conditions (1 M NaCl, Fig. 4). The salt concentration-dependent growth defect in the double mutant suggests that sensitivity to osmotic stress is a component of the synthetic growth defect. Importantly, this points to the presence of parallel cellular pathways that promote survival under osmotic stress, with one arm consisting of the HOG signaling pathway while the other arm is supported by V-ATPase function.

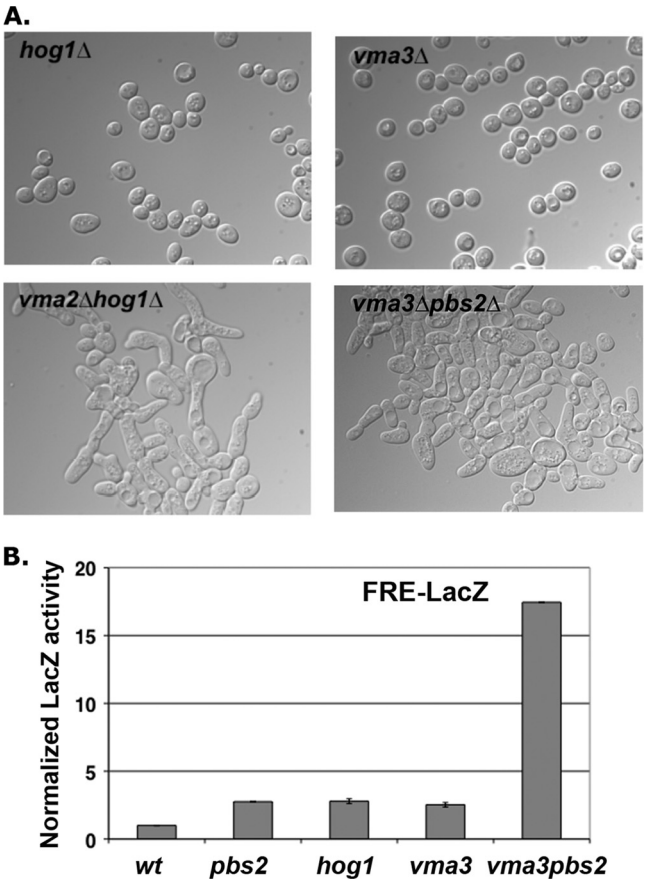

FIG 5 Phenotypic analysis of *hog1*Δ, *vma3*Δ, *vma2*Δ *hog1*Δ, and *vma3*Δ *pbs2*Δ haploids. (A) *vma2*Δ *hog1*Δ and *vma3*Δ *pbs2*Δ strains show an altered morphology on solid medium. Haploid single and double mutants were grown on YEPD (pH 5.0) plates at 25°C for 48 h. The cells were then visualized under an oil immersion objective at ×100 magnification. (B) Wild-type, *hog1*Δ, *pbs2*Δ, *vma3*Δ, and *vma3*Δ*pbs2*Δ strains were transformed with a plasmid bearing LacZ under the control of a FRE-containing promoter. The β-galactosidase activity was determined in suspensions of cells scraped from solid medium as described in Materials and Methods and normalized to the activity in wild-type cells. The means of three assays (± the standard errors of the mean) are shown for each sample.

Furthermore, these double mutant cells have an aberrant morphology characterized by long, filamentous, multipolar cells when grown on solid media (Fig. 5A). If transcriptional downregulation of mating and filamentous growth pathway genes in the *vma2*Δ mutant described above represents a suppression of cross talk between MAPK pathways when the HOG pathway is activated, then deletion of the terminal members of the HOG pathway in a *vma2*Δ mutant might allow cross-activation of other MAPK pathways (7,

18, 30). Double *vma2*Δ *hog1*Δ and *vma3*Δ *pbs2*Δ mutants do exhibit a filamentous morphology, particularly on solid medium, suggesting that cross-activation of the filamentous growth MAPK pathway may be occurring. We tested whether this pathway was activated in the double mutants using a pFRE-LacZ fusion (32). The filamentous growth pathway culminates in activation of the Tec1 transcription factor to transcribe genes containing FRE sequences (27). We assessed the β-galactosidase activity in strains transformed with a FRE-LacZ fusion plasmid by initially growing the cells on plates, where the morphological phenotype was most prominent, and then suspending them for activity measurements (32). As shown in Fig. 5B, the double mutant *vma3*Δ*pbs2*Δ shows a 17-fold-higher β-galactosidase activity than wild-type cells, indicating strong activation of the pFRE-LacZ in the double mutant. The *pbs2*Δ, *hog1*Δ, and *vma3*Δ single mutants all had activities that were ~2.5-fold that of the wild type. The results are consistent with activation of the HOG pathway in the *vma2*Δ mutant, leading to cross-activation of the filamentous growth pathway when the penultimate (Pbs2p) and terminal (Hog1p) kinases of the HOG pathway are deleted.

V-ATPase responds to external salt stress. The synthetic growth phenotype of *vma*Δ *hog*Δ double mutants suggests that V-ATPase function is required to handle salt stress. V-ATPases establish a proton gradient across the vacuolar membrane that allows the uptake of different cations into the vacuole by cation/H^+ antiporters (4). From this, we hypothesized that upon NaCl stress, the proton gradient drives Na^+ sequestration into the vacuole. Storage of Na^+ in the vacuole would thus provide a mechanism of Na^+ detoxification complementary to activation of Na^+ export and synthesis of osmoprotectants driven by the HOG pathway.

To test the importance of V-ATPases in yeast vacuoles for Na^+/H^+ exchange, we isolated vacuolar vesicles and established a steady-state pH gradient that was detected by ACMA quenching (Fig. 6). As shown in Fig. 6A, addition of Mg-ATP results in the establishment of a proton gradient, demonstrated by ACMA quenching, and the pH gradient is rapidly collapsed by the addition of high concentrations of the V-ATPase inhibitor concanamycin A. We first tested for Na^+/H^+ antiport by addition of NaCl (333 mM) to vacuoles in the absence of concanamycin A. If Na^+/H^+ antiporters were transporting Na^+ ions into the vacuole at the expense of the proton gradient, we would expect to see a rise in ACMA fluorescence (5, 51). We did not observe a reversal of ACMA quenching and instead saw a consistent small decrease in ACMA fluorescence. This suggests that the V-ATPase is able to maintain the proton gradient at the vacuole during salt shock but does not indicate whether Na^+/H^+ exchange has occurred. We next tested whether partial inhibition of the V-ATPase could allow us to observe Na^+/H^+ exchange via a change in ACMA quenching in response to excess NaCl (Fig. 6B and C). Again, we stimulated V-ATPase proton pumping by adding Mg-ATP at 100 s. We decreased the population of active V-ATPase molecules by adding subsaturating amounts of concanamycin (0.25 or 0.5 nM concanamycin A at 200 s) until a new steady-state level of ACMA fluorescence was achieved and subsequently added 333 mM NaCl to the same cuvette (400-s time point). Notably, we were able to observe an increase in ACMA fluorescence upon adding NaCl to vacuoles treated with either 0.25 or 0.5 nM concanamycin A (Fig. 6B and C, black circles). This reflects the influx of sodium ions into the vacuole, leading to the depletion of proton gradient

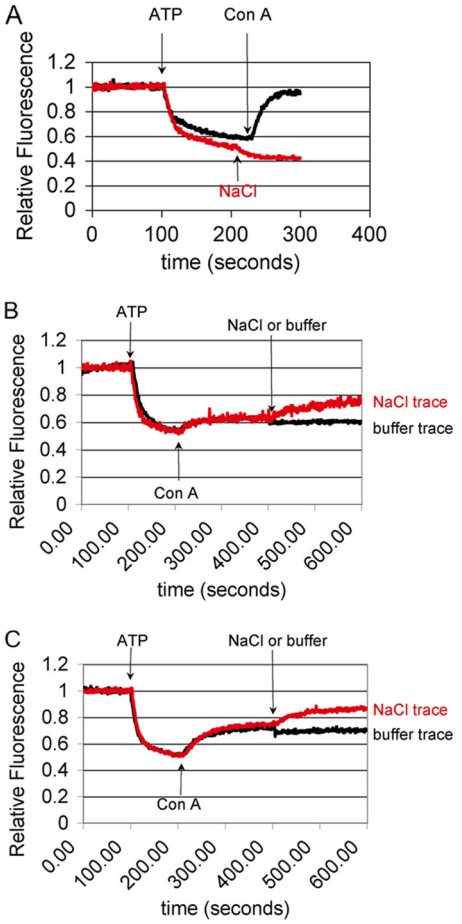

FIG 6 Excess NaCl can partially collapse the vacuolar H^+ gradient unless V-ATPase activity is maintained. For each set of plots, vacuolar vesicles were mixed with 1 μM ACMA in transport buffer (50 mM NaCl, 30 mM KCl, 20 mM HEPES [pH 7]). The fluorescence intensity was monitored continuously as the mixture was stirred at 25°C. For all traces, Mg-ATP was added at 100 s to initiate proton pumping. (A) Response of vacuoles to salt when the V-ATPase is not inhibited. After 200 s, 100 nM concanamycin A (black) or 333.33 mM NaCl (red) was added the cuvette. (B and C) Response of vacuoles to salt when the V-ATPase is partially inhibited by concanamycin A. For these traces, vacuoles were exposed to either 0.25 nM (B) or 0.5 nM (C) concanamycin A at 200 s. After treatment with these subsaturating amounts of concanamycin A, the vacuoles were exposed to 333.3 mM NaCl (red) or an equivalent amount of buffer (black) at 400 s.

by Na^+/H^+ antiporters (5). These results indicate that Na^+ influx into the cytosol might be partially countered by Na^+ uptake into the vacuole and that vacuolar uptake of Na^+ ions could deplete the vacuolar H^+ gradient without ongoing V-ATPase activity.

If V-ATPase activity is critical for maintenance of the proton gradient during salt stress, we reasoned that it might be activated in response to extracellular salt. We isolated vacuolar vesicles from wild-type cells exposed to high salt conditions (500 mM NaCl) for 30 min just before lysis and compared vacuolar vesicles purified from salt-shocked cells to those from cells exposed to typical salt concentrations in buffered medium (50 mM NaCl). Interestingly, vacuolar vesicles isolated from salt-stressed cells had ~65% higher V-ATPase activities than those purified from unstressed cells (Fig. 7A). This difference is comparable to the observed change in V-ATPase activity resulting from subjecting cells to glucose depri-

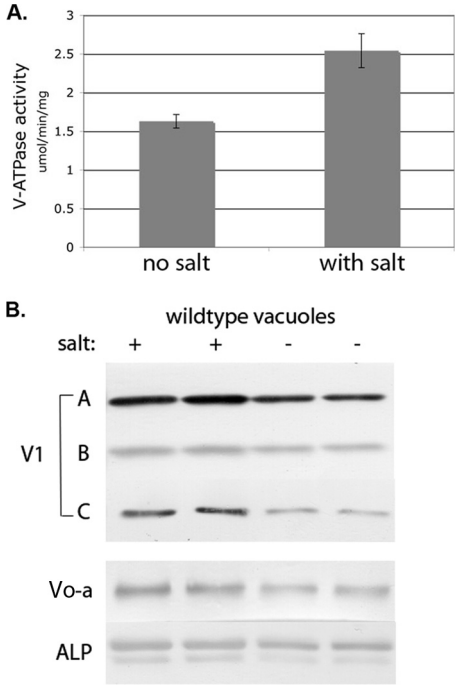

FIG 7 V-ATPase activity and V_1-V_o assembly in wild-type vacuoles isolated from salt-treated cells. Vacuolar vesicles were isolated as described in Materials and Methods from spheroplasts recovered for 30 min in the presence (+) or absence (−) of 500 mM NaCl. (A) Concanamycin A-sensitive ATPase specific activities (V-ATPase activity) were measured in vesicles from cells exposed or not exposed to 500 mM NaCl. (B) Equal amounts of vacuolar protein from each condition were separated on SDS-PAGE, and Western blotting was performed to visualize V_1 subunits (A, B, and C) and the V_o-a subunit. The levels of alkaline phosphatase, a vacuolar protein, were also visualized to ensure equal loading.

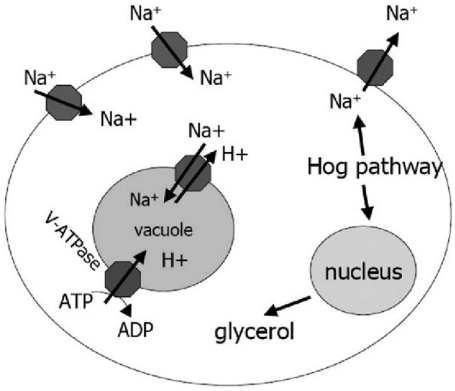

FIG 8 V-ATPase is important in salt detoxification during hyperosmotic stress. The HOG MAPK signaling pathway and the V-ATPase act in parallel pathways to mitigate osmotic shock during salt stress. Activation of the HOG pathway leads to changes in gene expression that promote production of glycerol, an osmoprotectant. The HOG pathway also activates transporters at the plasma membrane, resulting in the extrusion of NaCl into the extracellular space. On the other hand, the V-ATPase becomes activated in response to salt stress, and higher activation of the enzyme is required for the activity of vacuolar cation transporters that recruit excess sodium ions into the vacuolar lumen.

vation or high extracellular pH before vacuole isolation (9, 19). Western blot analysis of these vacuoles showed increased assembly of V_1 subunits A, B, and C with V_o sectors (represented by V_o-a subunit) in vacuoles from salt-stressed cells (Fig. 7B). As in other cases where V-ATPase assembly is regulated (9, 19), the difference in levels of V_1 subunit C is the most pronounced (9). These results indicate that increased V-ATPase activity during salt stress is derived from increased levels of V-ATPase assembly.

Given the data in Fig. 6, it appears that activation of the V-ATPase during salt stress conditions may support Na^+/H^+ exchange and prevent exhaustion of the vacuolar proton gradient. Salt activation of the V-ATPase underscores the functional importance of the enzyme during salt stress and provides biochemical support for the genetic interaction observed in the CHI screen.

DISCUSSION

Our results suggest that the V-ATPase and the HOG pathway may act in parallel to compensate for salt shock, as shown in Fig. 8. Based on the results discussed below, we propose that the HOG pathway promotes salt tolerance by supporting cytosolic osmolyte accumulation and cellular salt export through plasma membrane exchangers such as Nha1 (17) but that V-ATPase activation supports salt sequestration into the vacuole through exchangers dependent on the H^+ gradient. Loss of salt sequestration into organelles can be partially suppressed by constitutive activation of the HOG pathway, but V-ATPase function becomes essential under salt stress when the HOG pathway is compromised.

Genetic and functional interactions between the HOG pathway and the V- ATPase. The canonical response to osmotic shock involves the activation of the HOG MAPK signaling pathway. Significantly, despite many growth defects, *vma* mutants are not among the most salt-sensitive deletion mutants (16). We uncovered the link between the HOG pathway and the V-ATPase through a genomic CHI screen against V-ATPase subunits, which was initiated with the goal of looking for pathways and processes that require full V-ATPase function. This genetic interaction may uncover a requirement for V-ATPase function that is normally compensated for by a second pathway (15). A synthetic phenotype arising as a result of reducing the gene copy number of both a *VMA* gene and HOG pathway member suggests that at least one of the pathways must be fully functional for normal growth or that reducing the output of one pathway requires the other pathway to function at full capacity in compensation.

To determine the functional link between the HOG pathway and V-ATPase function, we characterized the ability of V-ATPase mutants to handle salt stress. *vma* mutants are sensitive to very high levels of osmotic/ionic stress (Fig. 4), reflecting a need for V-ATPase function in salt resistance, but our results suggest that the full importance of the V-ATPase in salt stress may be masked by compensatory activation of the HOG pathway even at relatively low-salt conditions (Fig. 3). It is particularly telling that there is more Hog1p phosphorylation in a *vma2*Δ mutant exposed to relatively low levels of osmotic stress (0.25 M NaCl) compared to a wild-type strain treated in a similar manner; this suggests that a loss of V-ATPase activity results in elevated cytosolic salt concentrations and increased HOG pathway activation. Interestingly, *PTP2*, a negative regulator of the HOG pathway, was also upregulated in a *vma2*Δ mutant; upregulation of this negative regulator likely tempers HOG pathway activation in the *vma2*Δ mutant (17). This again suggests that *vma2*Δ mutants experience significant osmotic stress. Although only a subset of the genes activated

by Hog1 in response to an acute salt stress are upregulated in a *vma2*Δ mutant, it should be noted that transcription of these genes is often only transiently induced in response to salt (33). Westfall et al. (49) have shown that genes directly involved in glycerol production may be the most important Hog1 transcriptional targets for long-term survival under salt stress; *GPD2*, which is upregulated in *vma2*Δ cells, falls into this category. Taken together, these results suggest that the HOG pathway is activated in order to cope with the loss of V-ATPase function and that, in wild-type cells, the V-ATPase works in parallel with the HOG pathways to help cells to cope with even relatively modest osmotic stress. Consistent with this, the *vma2*Δ *hog1*Δ double mutant haploid poorly tolerates exposure to salt (Fig. 4).

In addition to their severe synthetic growth phenotype, both *vma2*Δ *hog1*Δ and *vma3*Δ *pbs2*Δ haploid double mutants exhibit a striking morphological defect (Fig. 5A). These haploids are grossly elongated and form filament-like structures on solid media. In yeast, the osmotic stress, mating, and pseudohyphal growth MAPK pathways share common upstream components (38). Previous studies have shown that the deletion of the more specific downstream components can lead to cross talk or improper activation of another MAPK pathway (7, 30). In fact, mutations in Pbs2 and Hog1 (the MAPKK and MAPK of the HOG pathway) have been shown to cause the inappropriate activation of the pheromone response or filamentous growth pathways in the presence of osmotic stress (7, 30, 36). In the *vma2*Δ *hog1*Δ and *vma3*Δ *pbs2*Δ double mutants, upstream HOG pathway components are activated in the *vma2*Δ mutant, but this signal is unable to reach the terminal Pbs2 and Hog1 kinases, and this results in cross talk with the pseudohyphal/filamentous growth pathway, based on activation of FRE-LacZ transcription. Notably, a number of pheromone response genes are downregulated in the *vma2*Δ mutant relative to wild-type cells of the same mating type (see Table S3 in the supplemental material); it is possible that loss of downregulation of these genes by introducing an additional *PBS2* or *HOG1* deletion also contributes to the phenotype.

The importance of the V-ATPase during osmotic stress. Links between V-ATPase function and salt detoxification have previously been uncovered in plants (23, 34, 35, 44). Reduced V-ATPase activity leads to lower salt tolerance in plants (2, 23, 31). There is also evidence of increased V-ATPase activity in response to salt stress in a large number of plant species and tissues (reviewed in reference 44), but the mechanisms for increasing V-ATPase activity appear to vary, including transcriptional activation of V-ATPase subunits (26), upregulation of ATPase and proton pumping activities with no change in subunit levels (34), and direct or indirect activation by upstream signaling components, such as the SOS2 kinase in *Arabidopsis* (2). The results presented here indicate that in yeast, V-ATPase activity is upregulated by increasing assembly of V_1 subunits with V_o subunits at the vacuolar membrane in response to salt. We observed no increase in total cellular levels of V_1 or V_o subunits in response to high salt (data not shown). Instead, the activation of the V-ATPase in response to salt stress employs the same basic mechanism as V-ATPase activation upon glucose readdition and V-ATPase stabilization at high extracellular pH: increased recruitment or retention of cytosolic V_1 subunits at the vacuolar membrane (9, 21). These results add to the evidence that V-ATPase assembly and activity are regulated by signals other than glucose levels (9). In plants, it is possible that some of the upstream signals implicated in salt activation of V-ATPases also reversibly impact V_1 assembly on the tonoplast. The plant vacuole is notably more complex than the yeast vacuole because there are two H^+ pumps present, the V-ATPase and a H^+-pyrophosphatase (H^+-PPase). Recent data have suggested that at the plant vacuole, the H^+-PPase was more important for salt detoxification than the V-ATPase (23). In this context, it is significant that we observed salt activation of V-ATPases in isolated yeast vacuolar membranes. This response suggests an important role for vacuolar pumps in organisms that lack an alternative proton pump, and it is still possible that V-ATPases in endosomes also participate in the response to salt stress.

In summary, we have shown that the V-ATPase has an important role in cell survival during hyperosmotic stress. The HOG pathway is upregulated in mutants that have lost V-ATPase function, and this may compensate for loss of vacuolar acidification. During hyperosmotic shock, vacuolar acidification acts in parallel with the HOG pathway, and the V-ATPase becomes essential for cell viability under even modest osmotic stress when the HOG pathway is absent. V-ATPase activity is higher during salt stress; this may counteract depletion of the proton gradient by exchangers involved in Na^+ uptake. These studies have uncovered a requirement for vacuolar acidification in the yeast osmotic stress response that has been previously unappreciated.

ACKNOWLEDGMENTS

This study was funded by Public Health Service grant R01 GM50322 from National Institutes of Health to P.M.K.

We thank Maureen Tarsio for doing the Hog1-LacZ experiments, David Amberg for helpful discussions, the Amberg and Cross/Duncan labs for the use of instrumentation, and Paul Cullen for providing the pFRE-LacZ construct.

REFERENCES

1. **Amberg DC, Burke DJ, Strathern JN.** 2005. Methods in yeast genetics. Cold Spring Harbor Laboratory Press, Cold Spring Harbor, NY.
2. **Batelli G, et al.** 2007. SOS2 promotes salt tolerance in part by interacting with the vacuolar H^+-ATPase and upregulating its transport activity. Mol. Cell. Biol. **27**:7781–7790.
3. **Breuer W, Shvartsman M, Cabantchik ZI.** 2008. Intracellular labile iron. Int. J. Biochem. Cell Biol. **40**:350–354.
4. **Cagnac O, Aranda-Sicilia MN, Leterrier M, Rodriguez-Rosales MP, Venema K.** 2010. Vacuolar cation/H^+ antiporters of *Saccharomyces cerevisiae*. J. Biol. Chem. **285**:33914–33922.
5. **Cagnac O, Leterrier M, Yeager M, Blumwald E.** 2007. Identification and characterization of Vnx1p, a novel type of vacuolar monovalent cation/H+ antiporter of *Saccharomyces cerevisiae*. J. Biol. Chem. **282**:24284–24293.
6. **Cyert MS.** 2003. Calcineurin signaling in *Saccharomyces cerevisiae*: how yeast go crazy in response to stress. Biochem. Biophys. Res. Commun. **311**:1143–1150.
7. **Davenport KD, Williams KE, Ullmann BD, Gustin MC.** 1999. Activation of the *Saccharomyces cerevisiae* filamentation/invasion pathway by osmotic stress in high-osmolarity glycogen pathway mutants. Genetics **153**:1091–1103.
8. **Denis V, Cyert MS.** 2002. Internal Ca^{2+} release in yeast is triggered by hypertonic shock and mediated by a TRP channel homologue. J. Cell Biol. **156**:29–34.
9. **Diakov TT, Kane PM.** 2010. Regulation of vacuolar proton-translocating ATPase activity and assembly by extracellular pH. J. Biol. Chem. **285**:23771–23778.
10. **Dove SK, Dong K, Kobayashi T, Williams FK, Michell RH.** 2009. Phosphatidylinositol 3,5-bisphosphate and Fab1p/PIKfyve underPPIn endo-lysosome function. Biochem. J. **419**:1–13.
11. **Duex JE, Nau JJ, Kauffman EJ, Weisman LS.** 2006. Phosphoinositide 5-phosphatase Fig. 4p is required for both acute rise and subsequent fall in

stress-induced phosphatidylinositol 3,5-bisphosphate levels. Eukaryot. Cell **5**:723–731.
12. **Duex JE, Tang F, Weisman LS.** 2006. The Vac14p-Fig4p complex acts independently of Vac7p and couples PI3,5P2 synthesis and turnover. J. Cell Biol. **172**:693–704.
13. **Elble R.** 1992. A simple and efficient procedure for transformation of yeasts. Biotechniques **13**:18–20.
14. **Giaever G, et al.** 2002. Functional profiling of the *Saccharomyces cerevisiae* genome. Nature **418**:387–391.
15. **Haarer B, Viggiano S, Hibbs MA, Troyanskaya OG, Amberg DC.** 2007. Modeling complex genetic interactions in a simple eukaryotic genome: actin displays a rich spectrum of complex haploinsufficiencies. Genes Dev. **21**:148–159.
16. **Hillenmeyer ME, et al.** 2008. The chemical genomic portrait of yeast: uncovering a phenotype for all genes. Science **320**:362–365.
17. **Hohmann S.** 2002. Osmotic stress signaling and osmoadaptation in yeasts. Microbiol. Mol. Biol. Rev. **66**:300–372.
18. **Jacoby T, et al.** 1997. Two protein-tyrosine phosphatases inactivate the osmotic stress response pathway in yeast by targeting the mitogen-activated protein kinase, Hog1. J. Biol. Chem. **272**:17749–17755.
19. **Kane PM.** 1995. Disassembly and reassembly of the yeast vacuolar H^+-ATPase in vivo. J. Biol. Chem. **270**:17025–17032.
20. **Kane PM.** 2006. The where, when, and how of organelle acidification by the yeast vacuolar H^+-ATPase. Microbiol. Mol. Biol. Rev. **70**:177–191.
21. **Kane PM, Parra KJ.** 2000. Assembly and regulation of the yeast vacuolar H^+-ATPase. J. Exp. Biol. **203 Pt. 1**:81–87.
22. **Kellermayer R, Aiello DP, Miseta A, Bedwell DM.** 2003. Extracellular Ca^{2+} sensing contributes to excess Ca^{2+} accumulation and vacuolar fragmentation in a *pmr1*Δ mutant of *Saccharomyces cerevisiae*. J. Cell Sci. **116**:1637–1646.
23. **Krebs M, et al.** 2010. *Arabidopsis* V-ATPase activity at the tonoplast is required for efficient nutrient storage but not for sodium accumulation. Proc. Natl. Acad. Sci. U. S. A. **107**:3251–3256.
24. **Li SC, Kane PM.** 2009. The yeast lysosome-like vacuole: endpoint and crossroads. Biochim. Biophys. Acta **1793**:650–663.
25. **Liu M, Tarsio M, Charsky CM, Kane PM.** 2005. Structural and functional separation of the N-and C-terminal domains of the yeast V-ATPase subunit H. J. Biol. Chem. **280**:36978–36985.
26. **Low R, et al.** 1996. Early salt stress effects on the differential expression of vacuolar H^+-ATPase genes in roots and leaves of *Mesembryanthemum crystallinum*. Plant Physiol. **110**:259–265.
27. **Madhani HD, Fink GR.** 1997. Combinatorial control required for the specificity of yeast MAPK signaling. Science **275**:1314–1317.
28. **Mattison CP, Ota IM.** 2000. Two protein tyrosine phosphatases, Ptp2 and Ptp3, modulate the subcellular localization of the Hog1 MAP kinase in yeast. Genes Dev. **14**:1229–1235.
29. **Milgrom E, Diab H, Middleton F, Kane PM.** 2007. Loss of vacuolar proton-translocating ATPase activity in yeast results in chronic oxidative stress. J. Biol. Chem. **282**:7125–7136.
30. **O'Rourke SM, Herskowitz I.** 1998. The Hog1 MAPK prevents cross talk between the HOG and pheromone response MAPK pathways in *Saccharomyces cerevisiae*. Genes Dev. **12**:2874–2886.
31. **Padmanaban S, Lin X, Perera I, Kawamura Y, Sze H.** 2004. Differential expression of vacuolar H^+-ATPase subunit c genes in tissues active in membrane trafficking and their roles in plant growth as revealed by RNAi. Plant Physiol. **134**:1514–1526.
32. **Pitoniak A, Birkaya B, Dionne HM, Vadaie N, Cullen PJ.** 2009. The signaling mucins Msb2 and Hkr1 differentially regulate the filamentation mitogen-activated protein kinase pathway and contribute to a multimodal response. Mol. Biol. Cell **20**:3101–3114.
33. **Posas F, et al.** 2000. The transcriptional response of yeast to saline stress. J. Biol. Chem. **275**:17249–17255.
34. **Queiros F, et al.** 2009. Activity of tonoplast proton pumps and Na^+/H^+ exchange in potato cell cultures is modulated by salt. J. Exp. Bot. **60**:1363–1374.
35. **Rausch T, et al.** 1996. Salt stress responses of higher plants: the role of proton pumps and Na^+/H^+ antiporters. J. Plant Physiol. **148**:425–433.
36. **Rep M, Krantz M, Thevelein JM, Hohmann S.** 2000. The transcriptional response of *Saccharomyces cerevisiae* to osmotic shock. Hot1p and Msn2p/Msn4p are required for the induction of subsets of high osmolarity glycerol pathway-dependent genes. J. Biol. Chem. **275**:8290–8300.
37. **Rizzo JM, Tarsio M, Martinez-Munoz GA, Kane PM.** 2007. Diploids heterozygous for a vma13Delta mutation in *Saccharomyces cerevisiae* highlight the importance of V-ATPase subunit balance in supporting vacuolar acidification and silencing cytosolic V1-ATPase activity. J. Biol. Chem. **282**:8521–8532.
38. **Roberts CJ, et al.** 2000. Signaling and circuitry of multiple MAPK pathways revealed by a matrix of global gene expression profiles. Science **287**:873–880.
39. **Roberts CJ, Raymond CK, Yamashiro CT, Stevens TH.** 1991. Methods for studying the yeast vacuole. Methods Enzymol. **194**:644–661.
40. **Rupp S.** 2002. LacZ assays in yeast. Methods Enzymol. **350**:112–131.
41. **Sambade M, Alba M, Smardon AM, West RW, Kane PM.** 2005. A genomic screen for yeast vacuolar membrane ATPase mutants. Genetics **170**:1539–1551.
42. **Sheikh-Hamad D, Gustin MC.** 2004. MAP kinases and the adaptive response to hypertonicity: functional preservation from yeast to mammals. Am. J. Physiol. Renal Physiol. **287**:F1102–F1110.
43. **Shock TR, Thompson J, Yates JR, III, Madhani HD.** 2009. Hog1 mitogen-activated protein kinase (MAPK) interrupts signal transduction between the Kss1 MAPK and the Tec1 transcription factor to maintain pathway specificity. Eukaryot. Cell **8**:606–616.
44. **Silva P, Geros H.** 2009. Regulation by salt of vacuolar H^+-ATPase and H^+-pyrophosphatase activities and Na^+/H^+ exchange. Plant Signal Behav. **4**:718–726.
44a. **Thorner J, Westfall PJ, Ballon DR.** 2011. High osmolarity glycerol (HOG) pathway in yeast. Sci. Signal. (Connections map in the Database of Cell Signaling, as seen 23 December 2011). http://stke.sciencemag.org/cgi/cm/stkecm;CMP_14620.
45. **Thumm M.** 2000. Structure and function of the yeast vacuole and its role in autophagy. Microsc. Res. Tech. **51**:563–572.
46. **Tong AH, et al.** 2001. Systematic genetic analysis with ordered arrays of yeast deletion mutants. Science **294**:2364–2368.
47. **Warringer J, Hult M, Regot S, Posas F, Sunnerhagen P.** 2010. The HOG pathway dictates the short-term translational response after hyperosmotic shock. Mol. Biol. Cell **21**:3080–3092.
48. Reference deleted.
49. **Westfall PJ, Patterson JC, Chen RE, Thorner J.** 2008. Stress resistance and signal fidelity independent of nuclear MAPK function. Proc. Natl. Acad. Sci. U. S. A. **105**:12212–12217.
50. **Wurgler-Murphy SM, Maeda T, Witten EA, Saito H.** 1997. Regulation of the *Saccharomyces cerevisiae* HOG1 mitogen-activated protein kinase by the PTP2 and PTP3 protein tyrosine phosphatases. Mol. Cell. Biol. **17**:1289–1297.
51. **Xu K, Zhang H, Blumwald E, Xia T.** 2010. A novel plant vacuolar Na^+/H^+ antiporter gene evolved by DNA shuffling confers improved salt tolerance in yeast. J. Biol. Chem. **285**:22999–23006.